

# Angle-resolved photoemission spectroscopy of band tails in lightly doped cuprates

A. S. ALEXANDROV and K. REYNOLDS  
 Department of Physics, Loughborough University,  
 Loughborough LE11 3TU, United Kingdom

We amend ab initio strongly-correlated band structures by taking into account the band-tailing phenomenon in doped charge-transfer Mott-Hubbard insulators. We show that the photoemission from band tails accounts for sharp "quasi-particle" peaks, rapid loss of their intensities in some directions of the Brillouin zone ("Fermi arcs") and high-energy "waterfall" anomalies as a consequence of matrix-element effects of disorder-localised states in the charge-transfer gap of doped cuprates.

PACS numbers: 71.38.-k, 74.40.+k, 72.15.Jf, 74.72.-h, 74.25.Fy

Since the discovery of high- $T_c$  superconductivity in cuprates, angle-resolved photoemission spectroscopy (ARPES) has offered a tremendous advance into the understanding of their electronic structure [1]. However, even though ARPES is continually strengthening our insights into the band structure and correlations in cuprates, it has also revealed many poorly understood phenomena, such as the incoherent "background", the sharp "quasi-particle" peaks near some points of the Brillouin zone (BZ), which form "arcs" of "Fermi surface" (FS) [2] and references therein), widely studied low-energy dip-hump and kink features (for review see [1]) and the more recently discovered steep downturn of the dispersion toward higher energies (the so-called "waterfall") [3, 4, 5, 6, 7, 8]. These anomalies have received quite different interpretations, involving, for example, uncorrelated [10] and strongly-correlated [11, 12, 13, 14] lattice polarons, Middelhuisberg-like approaches [15, 16], spinons and holons [3], spin polarons [5], spin fluctuations [9, 17] and band-structure matrix element effects [8, 18].

Many ARPES interpretations suggest a large FS (as an exception see e.g. [10]) with nodal gapless quasiparticles, which are gapped or strongly damped in the antinodal directions  $(0;0)$  and  $(\pi;\pi)$  of the two-dimensional (2D) BZ. Importantly, extensive simulations of ARPES using the first-principles (LDA) band theory with thematrix elements properly taken into account [18] reproduces well the topological features of momentum distribution curves (MDC), pointing to the large FS in optimally doped cuprates. However, LDA predicts that the undoped parent cuprates are metallic with roughly the same large FS, while they are actually charge-transfer Mott-Hubbard insulators with the optical gap at 2 eV. This fact led to several powerful extensions of LDA, in particular to LDA+U, which combines LDA eigenfunctions with strong Coulomb correlations introduced as a model parameter (Hubbard U) [19], and the LDA+generalized tight-binding (GTB) method combining the exact diagonalization of the intracell part of the Hamiltonian with relevant LDA eigenfunctions and Coulomb correlations and the perturbation treatment of the intercell hoppings and interactions [20]. LDA+GTB Hamiltonian is reduced

to the simpler effective t-J or t-J model (t-J model plus three-center correlated hoppings [20]) in the low-energy domain.

LDA+GTB band structure of undoped cuprates with ab initio sets of tight-binding parameters [20] describes remarkably well the optical gap,  $E_{ct} \approx 2$  eV both in antiferromagnetic and paramagnetic states of the undoped  $\text{La}_2\text{CuO}_4$ . The valence band consists of a set of very narrow ( $\approx 1$  eV) subbands where the highest one is dominated by the oxygen p states with the maximum at  $k = g = (\pi/2a, \pi/2a)$  (see Fig.1), while the bottom of the empty conduction band formed by  $d_{x^2-y^2}$  states of copper is found at  $(0;0)$ . These locations of valence-band maximum and conduction-band minimum perfectly agree with ARPES intensity locus in hole-doped  $\text{La}_{2-x}\text{Sr}_x\text{CuO}_4$  and electron-doped  $\text{Nd}_{2-x}\text{Ce}_x\text{CuO}_4$ , respectively [21]. Importantly, the LDA+GTB approach predicts the charge-transfer gap at any doping with the chemical potential pinned near the top of the valence band (in hole-doped cuprates) and near the bottom of the conduction band (in electron-doped cuprates) due to spin-polaron in-gap states.

ARPES of undoped cuprates [1, 2, 21] proved to be critical in the assessment of different theoretical approaches. It revealed an apparent contradiction with the t-J model. There is no sharp peak predicted by the model in undoped cuprates, but a slightly dispersive broad incoherent background, Fig.2 (inset). Small lattice polarons due to a strong electron-phonon interaction (EPI) have been advocated as a plausible explanation of the discrepancy [12]. When EPI is strong, the spectral weight,  $Z$ , of the coherent small-polaron peak is very small,  $Z \ll 1$  and, hence the peak can not be seen in experiment since all weight of the sharp resonance in the t-J model is transformed at strong EPI into the broad continuum.

Unfortunately the energy distribution curves (EDC), Fig.2a,b, has only little if any resemblance to the small-polaron spectral function, which is roughly gaussian-like. Only by subtracting a "background" given by the spectrum near  $(0;0)$ , Fig.2, one can account for the remaining EDC with the polaronic spectral function [14]. This background problem obscures any reliable interpre-

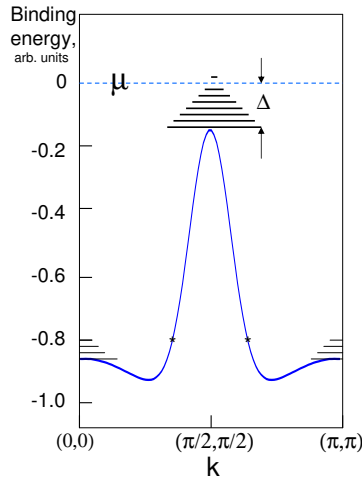


FIG. 1: LDA + G TB valence band dispersion [20] am ended with band tails (ladder lines) near  $\pm(\pi/2, \pi/2)$  and  $\pm(\pi, \pi)$  maxima (here  $k$  is measured in  $1/a$ )

tation of the broad ARPES intensities, especially in underdoped cuprates, where the charge-transfer gap at 2 eV makes inelastic scattering events plausible as an explanation of the background. Sharp peaks at  $(\pm 2a, \pm 2a)$  near the Fermi level, Fig. 2b, in doped cuprates also remains a puzzle. Small heavy polarons cannot screen EPI in lightly doped cuprates. Hence, if  $Z$  is small in the parent cuprate, it should also remain small at finite doping, so that the emergence of the peaks cannot be explained by a substantial increase of  $Z$  with doping.

Here we show that am ending the LDA + G TB band structure of doped cuprates by inevitable impurity band-tails, the ARPES puzzles as mentioned above are explained.

Doping of cuprates inserts a large number of impurities into the parent lattice. Each impurity ion locally introduces a distinct level,  $E_i$ , in the charge-transfer gap. The fact that the impurities are randomly distributed in space causes the density of states (DOS) to tail, like in heavily doped semiconductors [22]. When there are many impurities within the range  $\pm a$  of a localised wave function  $\phi_i(r)$ , the random potential produces low-energy states near maxima of the valence band at hole doping, Fig. 1, or near minima of the conduction band at electron doping. As a result, ARPES intensity,  $I(k; E) = I_b(k; E) + I_{im}(k; E)$  comprises the band-tail intensity,  $I_{im}(k; E)$ , due to localised states within the charge-transfer gap, and the valence band contribution,  $I_b(k; E)$ , of itinerant Bloch-like states. According to LDA band structures [18] the itinerant states are anisotropic 3D (specifically in  $\text{La}_2\text{CuO}_4$ ) dispersing with  $c$ -axis  $k_z$

over a few hundred meV. We suggest that this dispersion shapes the background making it so different from the incoherent background caused by EPI and/or spin fluctuations since  $k_z$  is not conserved in ARPES experiments.

Here we focus on the band-tailing contribution described by the Fermi-Dyadic golden rule as

$$I_{im}(k; E) = \frac{2e^2}{m_e^2} n(E) \sum_i \hbar f_i A_0 \frac{r}{\lambda} \frac{1}{(E + E_i)^2} \quad (1)$$

We define all energies relative to the chemical potential,  $\mu$ , which is situated within the impurity band as shown in Fig. 1. Only the impurity states with the binding energy  $E_i$  below  $\mu = 0$  contribute at zero temperature. Here  $A_0$  is the amplitude of X-ray vector potential, and  $\lambda = k_B = 1$ .

We take the impurity wavefunction as [23],  $\phi_i(r) = F_i(r) g_i(r)$ , and the final state to be the normalised plane wave,  $f_i(r) = (N v)^{1/2} \exp(i k_i r)$ . Here  $g_i(r)$  is the itinerant state at the top of the valence band,  $F_i(r)$  is a slowly varying envelope function, and  $N$  is the number of unit cells of volume  $v$  in the crystal. In the framework of GTB [20] one can expand  $g_i(r)$  using the Wannier orbitals,  $g_i(r) = N^{1/2} \sum_m w_m(r) \exp(i q_m r)$ , and calculate the dipole matrix element in Eq. (1) as

$$I_{im}(k; E) = I n(E) \sum_i f_i(k) g_i^2(E + E_i); \quad (2)$$

where  $I = 2(d/m_e)^2 (A_0 \lambda)^2 v$  is proportional to the valence band matrix element squared, which is roughly a constant in a wide range of  $k$  near RG,  $d = dr w(r) \exp(i q r)$ , and  $f_i(q) = (N v)^{1/2} dr \exp(i q r) F(r)$  is the Fourier transform of the impurity envelope function.

Since the size of the envelope is large compared with the lattice constant, its Fourier transform strongly depends on  $q$ , which explains the experimental EDC and MDC as we show in the rest of the paper. We choose the impurity state to be hydrogen-like,  $F_i(r) = (N v)^{1/2} \exp(-r/a_i)$  as the hydrogen model accurately predicts many properties of shallow levels in heavily doped semiconductors, so that  $f_i(q) = 8 (a_i^3 = N v)^{1/2} (1 + q^2 a_i^2)^{-3/2}$  for 3D impurity states, and  $f_i(q) / (1 + q^2 a_i^2)^{3/2}$  for 2D states like localised surface states. It is important to recognise here that  $a_i$  is related to the impurity binding energy as  $a_i^2 = m E_i$ , where  $m$  is roughly the hole effective mass. As a result we get  $I_{im}(k; E) = x I n(E) M(k) g_i^2(E)$  with

$$M(k) g_i^2(E) = \frac{64}{v m} \frac{(E + E_i)^{5/2}}{(E + E_i + (k - q)^2/m)^4} I_{im}(E + E_i); \quad (3)$$

Here  $I_{im}(E) = N_i^{-1} \sum_i (E - E_i)$  is the band-tail density of states (DOS) normalised to unity, and  $x = N_i N$  is the impurity concentration per cell proportional to doping. In the 2D case the result is similar,  $M_{2D}(k; E) / (E + E_i)^2 (E + E_i + (k - q)^2/m)^3 I_{im}(E + E_i)$ .

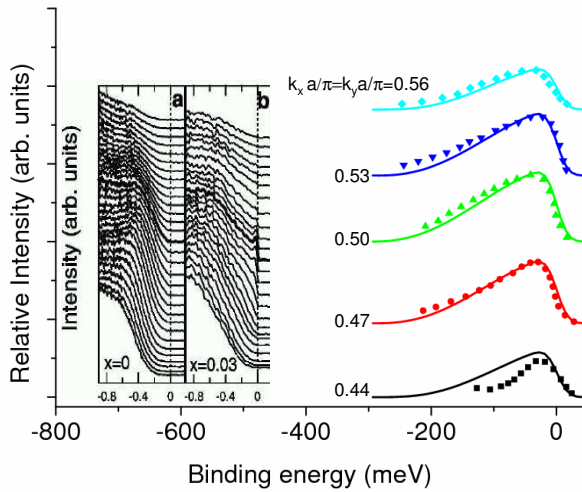


FIG. 2: Band-tail EDC, Eq.(4), (solid lines) with pseudogap  $\Delta = 300$  m eV and band-tail width  $\gamma = 300$  m eV compared with relative EDC (symbols) near  $(\mathbf{k} = 2a; \mathbf{g} = 2a)$ . Relative intensities are obtained by subtracting ARPES intensities of the parent compound,  $\text{La}_2\text{CuO}_4$  (a), shifted by  $\gamma$ , from EDC of slightly doped  $\text{La}_{1.97}\text{Sr}_{0.03}\text{CuO}_4$  (b) as measured by Yoshida et al [2]. Both intensities have been normalized by their values at  $E = -800$  m eV and the chemical potential shift between two samples has been taken as  $\gamma = 70$  m eV.

We notice that due to a very sharp dependence on  $\mathbf{g}$  of the matrix element in Eq.(2) any uncertainty of  $k_z$  does not smear out the strong dependence of  $I_{\text{im}}(\mathbf{k}; E)$  on the in-plane momentum component,  $k_x$ . Averaging over  $k_z$  simply replaces  $M(\mathbf{k} = \mathbf{g}; E)$  in Eq.(3) by

$$M'(\mathbf{k} = \mathbf{g}; E) = \frac{32c}{\pi m} \frac{(E + \gamma)^{5/2}}{[(E + \gamma + (k_x - g)^2/m)^{7/2}]^{im}(E + \gamma)};$$

where  $c$  is the  $c$ -axis lattice constant. Also  $M$  and  $M'$  can be very large for shallow impurity states,  $M \gg M'$  ( $1 \gg x$ ). Hence even the strong polaronic reduction of their weight,  $Z \ll 1$ , does not make band-tails invisible in ARPES at finite doping, in contrast to a complete reduction of the coherent band peak.

Since the chemical potential shifts towards the band edge with doping,  $\gamma$  in Eqs.(3,4) becomes smaller. Hence, the band-tail peak,  $I_{\text{im}}(\mathbf{k}; E)$ , which is proportional to  $x$ , not only increases but also becomes sharper with doping as observed [2]. To provide more insight into the shape and momentum dependence of experimental EDC we approximate the band-tail DOS by the simple form,  $I_{\text{im}}(E) = [h = (p=n+1-n)](E-\gamma)^p \exp(-|E-\gamma|^n)$ , where  $\gamma(x)$  is the gamma-function. Exponents  $n, p$  depend on the dimensionality and the correlation length of the disorder potential:  $n = 2$  both in 2D and 3D,  $p = 2$  in 2D and  $p = 7/2$  in 3D for the long range random poten-

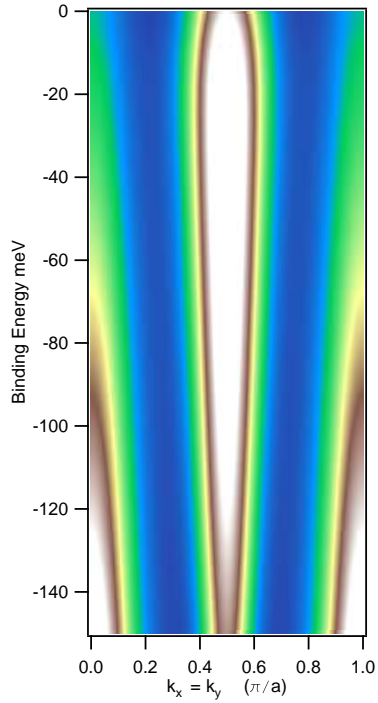


FIG. 3: Waterfall effect in the band-tail ARPES intensity (white colour corresponds to the highest intensity).

tial correlations. In the short-range Gaussian-white-noise limit one obtains  $n = 1, 1/2$  in 2D and 3D, respectively, and  $p = 3/2$  in both dimensions [24]. We can separate impurity and band contributions by subtracting normalized ARPES intensity of the parent cuprate from the intensity of the doped one. Then, the band-tail ARPES, Eq.(4), fits well with the experimental relative intensities at all momenta around  $\mathbf{g}$  with  $m = m_e$ ,  $n = 2$ , and  $p = 7/2$ , Fig.2. It describes the substantial loss of intensity with changing the momentum by only a few percent relative to  $\mathbf{g}$ , as well as the shape of the relative EDC.

We argue that band-tailing is also responsible for the waterfall effect. There are impurity tails near local maxima of the LDA+G+TB valence band at point  $(0;0)$  and at  $\mathbf{g}_1 = (\gamma = a; \gamma = a)$ , as shown in Fig.1. Different from in-gap impurity states at  $\mathbf{g} = (\gamma = 2a; \gamma = 2a)$  these localised states are hybridised with the valence band states of the same energy (shown by stars in Fig.1). However, the hybridisation could be insignificant, if the corresponding matrix elements of the random potential are small due to a large momentum separation between those states of the order of  $\gamma = 2a$ . Hence, the impurity peaks reappear and disperse towards  $(0;0)$  and  $\mathbf{g}_1$  at high binding energies, as observed in a number of doped cuprates [3, 4, 5, 6, 7, 8]. We illustrate the waterfall in Fig.3 by adding all three tail contributions,  $I_{\text{im}}(\mathbf{k}; E) / n(E) M'(\mathbf{k}_k; E + E_2) + M'(\mathbf{k}_k - \mathbf{g}; E) + M'(\mathbf{k}_k + \mathbf{g}_1; E + E_2)$  where  $E_2$  is roughly the valence band-width (we chose  $E_2 = 500$  m eV). We notice that the Fermi distribution,  $n(E)$ , is replaced by its convolution with the Gaussian

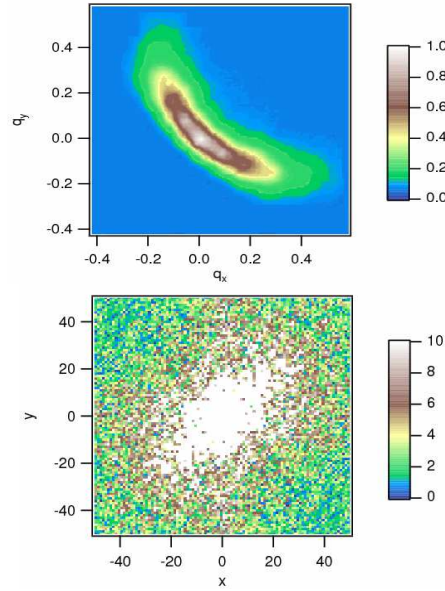


FIG. 4: Real space Fourier transform (lower panel) of the square root of ARPES intensities (arb. units) at the Fermi level (upper panel, measured by Yoshida et al. [2]) reveals the real-space size (in units of  $a$ ) of localised in-gap states.

sian energy resolution function,  $n(E) = [\text{erf}(E/\Delta) - \text{erf}(E_0/\Delta)]/2$  in plotting Figs 2,3 since the energy resolution  $\Delta = 20$  meV is much larger than  $T = 2$  meV.

Our theory proposes that the ARPES intensity near  $(\vec{q} = 2a, \vec{q} = 2a)$  is proportional to the square of the Fourier component,  $f_i(\vec{q})$ , of the impurity wave-function envelope,

Eq.(2). Therefore, we can find the real-space image of the function,  $F_i(r)$ , by taking the Fourier transform of the square root of the experimental intensities, Fig.4 (upper panel), [2]. The real-space image (lower panel, Fig.4) reveals some band-mass anisotropy and the size of the localised state of about 20 lattice constants justifies the "envelope" approximation [23] used for the impurity wavefunction.

In summary, we have proposed an explanation for sharp "quasi-particle" peaks, "Fermi arcs", and the high-energy waterfall in doped cuprates as a consequence of matrix-element effects of disorder-localised band-tails in the charge-transfer gap of doped Mott-Hubbard insulators. Importantly if holes are bound into bipolarons, the chemical potential remains within the single-particle band-tail at the bipolaron mobility edge even up to optimum doping, in agreement with S-N-S tunnelling experiments [25] and insulating-like low-temperature resistivity of underdoped cuprates. In this case in Fig.1 is half of the bipolaron binding energy [10], which is also the normal state pseudogap [26]. Recent scanning tunnelling microscopy at the atomic scale found intense nanoscale disorder in high-T<sub>c</sub> superconductor Bi<sub>2</sub>Sn<sub>2</sub>CaCu<sub>3</sub>O<sub>8+</sub> [27] telling us that band-tailing indeed plays the important role in shaping single-particle spectral functions of doped Mott insulators.

We are grateful to ZX Shen and Teppei Yoshida for providing us with their raw ARPES data [2] and enlightening comments. We greatly appreciate valuable discussions with Arun Bansil, Sergey Borisenko, Ivan Bozovic, Jim Hague, Jan Jung, Alexander Kordyuk, Maxim Korshunov, and Jan Zaanen. This work was supported by EPSRC (UK) (grant number EP/C518365/1).

---

[1] A. D'Amascelli, Z. Hussain and Zhi-Xun Shen, *Rev. Mod. Phys.* 75, 473 (2003); X. J. Zhou et al., cond-mat/0604284.

[2] T. Yoshida et al., *Phys. Rev. Lett.* 91, 027001 (2003).

[3] J. G. Rie et al., *Phys. Rev. Lett.* 98, 067004 (2007).

[4] W. M. Vevasana et al., cond-mat/0612541.

[5] B. P. Xie et al., cond-mat/0607450

[6] Z.-H. Pan et al., cond-mat/0610442.

[7] J. Chang et al., cond-mat/0610880.

[8] A. A. Kordyuk et al., cond-mat/0702374.

[9] A. M. Acridin et al., cond-mat/0701429.

[10] A. S. Alexandrov and C. J. Dent, *Phys. Rev. B* 60, 15414 (1999); A. S. Alexandrov and C. Srichewin, *Europhys. Lett.* 58, 576 (2002).

[11] G. Wellein, H. Roder, and H. Fehske, *Phys. Rev. B* 53, 9666 (1996).

[12] A. S. Mishchenko and N. Nagaosa, *Phys. Rev. Lett.* 93, 036402 (2004).

[13] M. Hohenadler et al., *Phys. Rev. B* 71, 245111 (2005).

[14] O. Rösch et al., *Phys. Rev. Lett.* 95, 227002 (2005).

[15] J. P. Hague, *J. Phys.: Condens. Matter* 15, 2535 (2003).

[16] E. G. Maksimov, O. V. Dolgov, and M. L. Kulic, *Phys. Rev. B* 72, 212505 (2005).

[17] S. V. Borisenko et al., *Phys. Rev. Lett.* 96, 117004 (2006).

[18] M. Lindroos, S. Sahrakorpi, and A. Bansil, *Phys. Rev. B* 65, 054514 (2002).

[19] V. I. Anisimov, J. Zaanen, and O. K. Andersen, *Phys. Rev. B* 44, 943 (1991).

[20] S. G. Ovchinnikov et al., *J. Phys.: Condens. Matter* 16, L93 (2004); M. M. Korshunov et al., *Phys. Rev. B* 72, 165104 (2005).

[21] K. M. Shen et al., *Phys. Rev. B* 69, 054503 (2004).

[22] P. V. Meighem, *Rev. Mod. Phys.* 64, 755 (1992).

[23] W. Kohn and J. M. Luttinger, *Phys. Rev.* 97, 869-883 (1955).

[24] B. I. Halperin and M. Lax, *Phys. Rev.* 148, 722 (1966); R. Eymard and G. Duraour, *J. Phys. D: Appl. Phys.* 6, 66 (1973); D. N. Quang and N. H. Tung, *Phys. Stat. Sol. B* 209, 375 (1998).

[25] I. Bozovic et al., *Nature (London)* 422, 873 (2003).

[26] A. S. Alexandrov, in *Studies in High Temperature Superconductors*, ed. A. V. Narlikar (Nova Science Pub., NY 2006), 50, pp. 1-69.

[27] J. Lee et al., *Nature (London)*, 442 546 (2006).